Science of the Total Environment 1047 (2026) 181973

Contents lists available at ScienceDirect

Science of the Total Environment

journal homepage: www.elsevier.com/locate/scitotenv

Research Paper

Decoding seasonal urban heat dynamics at neighborhood-scale using explainable deep learning for climate-resilient, digital twin-ready green planning

Priyanka Rao *, Patrizia Tassinari, Daniele Torreggiani

University of Bologna, Bologna, 40127, Emilia-Romagna, Italy

HIGHLIGHTS

- Seasonal LST patterns are shaped by multiple urban parameters.
- Neighborhood-scale LST drivers quantified using explainable modeling.
- XAI-enabled deep learning showed the best results among regression benchmarks.
- Built surface observed as the dominant temperature driver across seasons.
- Findings support data-driven Digital Twin systems for climate-resilient design.

GRAPHICAL ABSTRACT

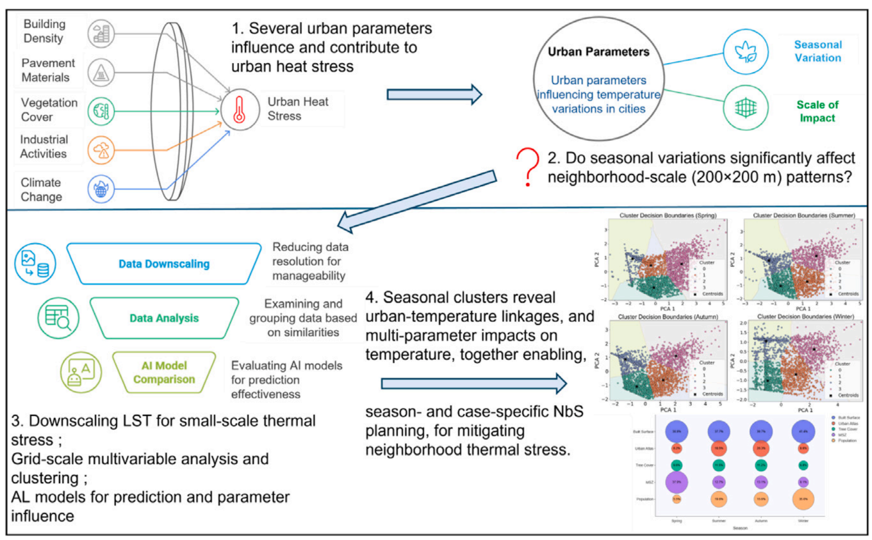

ARTICLE INFO

Keywords:
Seasonal LST
Urban morphology
Remote sensing
Explainable AI
Deep learning
Digital twin

ABSTRACT

Understanding the spatiotemporal dynamics of urban surface temperatures is essential for climate-resilient green planning under intensifying heat stress and rapid land-use change. This study investigates seasonal thermal behavior at a microscale analytical resolution (200 × 200 m) across Bologna, a densely urbanized city with diverse morphology. Satellite-derived land surface temperature (LST) was statistically downscaled to 10 m resolution and subsequently aggregated to the 200 m grid, and integrated with urban morphological and socioeconomic variables, including built surface, tree cover, population density, land-use classes, and settlement zones. A twofold approach was developed: (1) unsupervised k-means clustering to identify thermally distinct clusters per season, revealing consistent spatial patterns where tree-dominated areas remain cooler and dense urban cores warmer; and (2) an explainable deep learning model based on a convolutional neural network (CNN) to quantify variable contributions using permutation-based feature importance, benchmarked against Support Vector Machine, Random Forest, and XGBoost models. Model performance differences were evaluated using paired statistical tests with significance assessed at accepted thresholds. The CNN demonstrated competitive performance, effectively capturing nonlinear relationships in the data and, when combined with

* Corresponding author.
E-mail address: priyanka.rao2@unibo.it (P. Rao).

https://doi.org/10.1016/j.scitotenv.2026.181973
Received 22 November 2025; Received in revised form 7 June 2026; Accepted 18 June 2026
Available online 4 July 2026

subsequent analysis, providing insights into feature relevance. Built surface was the most influential driver (>37% across all seasons), while tree cover (7%–11%) and population density (5%–35%) showed pronounced seasonal variability, reflecting shifts in vegetation activity and energy demand. This integrative, interpretable modeling framework establishes a foundational step toward a neighborhood-scale urban climate digital twin, capable of linking multi-source data to simulate and explain intra-annual heat dynamics. The findings provide critical insights for adaptive, fine-scale heat mitigation and climate-resilient urban green planning.

1. Introduction

Urbanization, as a major driver of land-use change, has profoundly altered the physical and thermal characteristics of cities. The replacement of natural landscapes with impervious surfaces intensifies the urban heat island (UHI) effect (Yang et al., 2017b; Rao et al., 2023), which is further aggravated by global warming and significantly impacts urban livability and sustainability. Elevated surface temperatures increase risks to human health, energy demand, and productivity, particularly during extreme heat events (Tehrani et al., 2024; Wong et al., 2017). The interplay between temperature, urban morphology, and vegetation cover has been widely recognized as a key determinant of heat retention and distribution (Rao et al., 2021a,b, 2023; Wang et al., 2022). However, these relationships are inherently complex and often nonlinear, which traditional statistical approaches fail to capture (Marey et al., 2025) limiting their direct applicability for interpretable urban planning (Y. Zhang et al., 2025; Rao et al., 2023). While machine learning methods have been introduced to model such interactions, the combined influence of geospatial and morphological factors at the microscale level remains insufficiently explored (Zhou et al., 2022). Moreover, most existing models offer limited interpretability, which hinders their practical integration into planning workflows.

Advancements in remote sensing technologies have established satellite imagery as a central tool for analyzing UHI dynamics and mitigation strategies (Xu et al., 2022). Various studies have investigated intra-urban thermal variability and its relationship with land cover, demonstrating that thermal conditions differ significantly within cities due to their heterogeneous structures (Rao et al., 2023). To address this, frameworks such as Local Climate Zones (LCZs) classify urban landscapes into standardized categories, while resources such as the Copernicus Urban Atlas (European Commission and European Environment Agency, 2020) provide detailed maps to support urban planning. Although deep learning has enhanced the prediction of urban thermal patterns, most models remain opaque, thereby limiting their relevance for planning applications. Incorporating explainable AI (XAI) techniques offers a pathway to uncover the relative influence of environmental, morphological, and socio-economic factors, improving transparency and decision support for climate-responsive planning. Therefore, within compact modern cities, understanding how urban forms, urban design, green spatial patterns, and social factors collectively affect the spatial heterogeneity of the thermal environment at a small scale has become a major issue for planning sustainable living environments (Zhang et al., 2017).

Despite these advancements, urban–rural comparisons and broad classifications remain insufficient for capturing the subtle but critical variations in surface temperature across different urban morphologies. Land surface temperature (LST), derived from satellite observations, is a widely used indicator of the urban thermal environment. Vegetation and water bodies consistently lower LST, while impervious surfaces such as buildings and roads elevate it (Rao et al., 2023, 2024b). Beyond composition, spatial configuration, such as patch density, edge density, and shape complexity, also influences surface heat flux and energy exchange (Zhang et al., 2022). Although these 2D landscape metrics have revealed useful insights, they overlook the effects of vertical morphology. Building height, density, sky view factor (SVF), and facade area index (FAI) have been identified as critical predictors of surface temperature (Li et al., 2021). To contextualize the methodological approach adopted in this study, explicit three-dimensional geometric metrics were not incorporated due to the absence of spatially consistent high-resolution building morphology datasets across the entire domain. Instead, Morphological Settlement Zones (MSZ), used in conjunction with Urban Atlas land-use data, were employed as a scale-compatible proxy representation of urban form. MSZ classifications reflect typologies derived from built density, spatial layout, and generalized height classes, thereby capturing aggregated vertical–horizontal morphological structure relevant to neighborhood-scale thermal variability. While this proxy does not resolve fine-scale geometric processes such as canyon aspect ratios or detailed radiative exchange governed by SVF or FAI, it provides a consistent morphological characterization aligned with the spatial resolution and objectives of the present analysis. Moreover, the use of standardized, widely available datasets enhances methodological transferability and facilitates replication of the analytical framework across different urban contexts. From a broader literature perspective, relationships between vertical morphology indicators and surface temperature remain inconsistent: some studies suggest higher SVF increases solar heat gain (Berger et al., 2017), while others believe it enhances ventilation and reduces heat (Huang and Wang, 2019). It has been found that seasonality also plays a critical role in shaping the relationship between urban characteristics and LST, as variations in vegetation cover, solar radiation, and hydrothermal conditions alter their influence across different times of the year (Cheung et al., 2020; Hu et al., 2020). Studies show that biophysical parameters such as NDVI and NDBI exert stronger effects in warmer seasons, while building morphology indicators (e.g., height and structural variation) become more relevant during cooler periods (Hu et al., 2022). In addition, human activity patterns, often represented through urban functional zones (UFZs), create distinct thermal regimes due to uneven anthropogenic heat release (J. Chen et al., 2022). Although progress has been made, the seasonal variability of LST drivers and their differing impacts in the urban environment remain insufficiently explored, highlighting the need for comprehensive multi-season analyses.

In addition, the reliance on Landsat-derived LST at 30 m is one of the key limitations for small-scale urban thermal assessments. While widely used, this resolution blurs fine-scale thermal signatures and restricts the ability to capture localized effects of detailed morphology. Consequently, the relationship between urban form and LST remains unclear, and the influence of fine-scale heterogeneity is often overlooked (Du et al., 2022; Han, 2023). To mitigate this constraint, the present study employs statistical downscaling to derive higher-resolution LST estimates. The downscaled product was evaluated against the original Landsat-derived LST to ensure preservation of spatial thermal structure and radiometric consistency. However, this comparison does not constitute independent validation because the downscaled estimates are derived from the same source dataset, which and may introduce methodological circularity. In the absence of spatially distributed ground-based surface temperature observations or alternative high-resolution thermal imagery, Landsat observations were used as the most consistent spatially continuous reference available for evaluating pattern coherence in the downscaled estimates. Similar approaches have been adopted in previous downscaling studies (Zhou et al., 2016; Yang et al., 2017a) when independent validation data were unavailable. Moreover, classical regression models frequently employed in such analyses assume linear relationships, which are inadequate for representing the complex, nonlinear interactions among multiple urban variables (Wang et al., 2022). These methodological

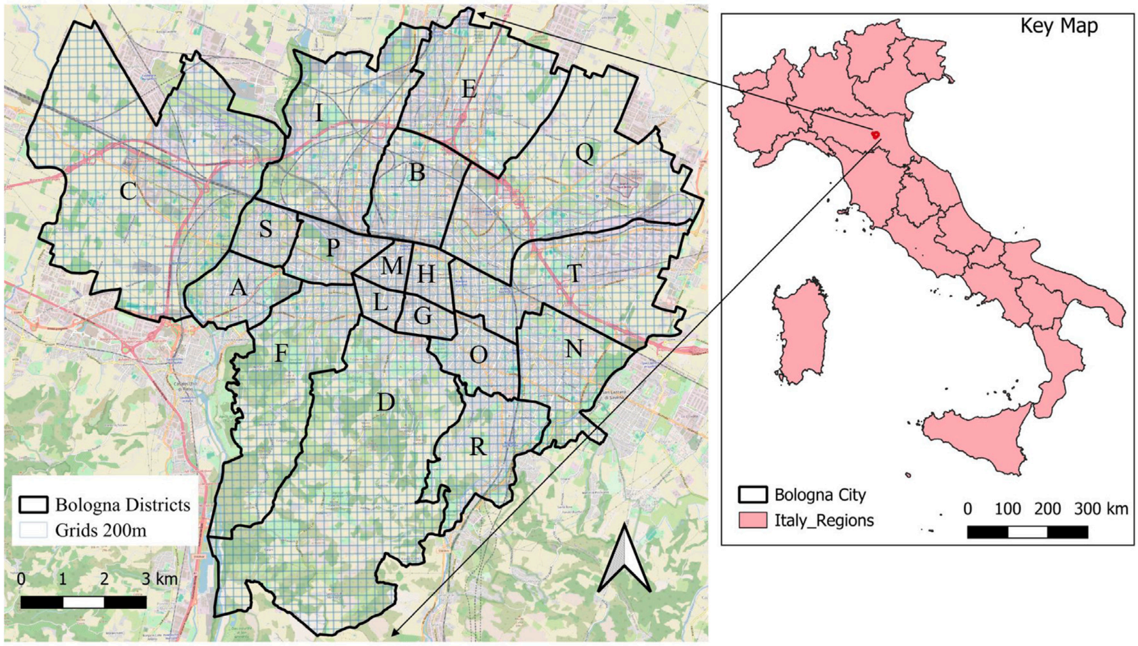

Fig. 1. Study Area Map, divided into grids and a total of 18 district boundaries with codes. The district boundaries have been retrieved from the regional geoportal of Emilia-Romagna (Emilia-Romagna Regional Geoportal, 2018).

and data limitations constrain the development of effective climate-responsive urban design strategies. High-resolution, multi-source modeling frameworks increasingly form the foundation of emerging urban climate digital twin concepts, which aim to fuse spatial data with predictive analytics for continuous assessment and scenario-based planning.

To address these gaps, this study investigates the urban thermal environment of Bologna, a highly urbanized city in the Emilia-Romagna region of Italy. A 200 *x* 200 m grid framework was applied (Yuan et al., 2024) to consistently evaluate fine-scale thermal variations and capture the combined influence of urban morphology, land-use characteristics, greenery, and socio-economic indicators. The study pursued two principal objectives: (1) to conduct a microscale seasonal analysis of neighborhood thermal patterns using unsupervised clustering of land surface temperature, pervious cover, impervious cover, and population; and (2) to quantify the seasonal contributions of morphological, environmental, and socio-economic variables to LST using a comparative machine learning framework. Specifically, the modeling target corresponds to the seasonal median LST aggregated at the 200 × 200 m grid-cell level, while predictor variables include built surface fraction, tree cover proportion, population density, and categorical urban morphology and land-use descriptors derived from MSZ and Urban Atlas datasets. By incorporating explainable deep learning techniques, the study provides interpretable insights into the drivers of urban heat and establishes a foundation for future neighborhood-scale urban climate digital twin frameworks.

The following sections of the paper are as follows: Section 2 consist of details about the study area and methodology applied. Further, Section 3 consists of the results, followed by sections 4 of discussions and 5 of conclusions.

2. Materials and methods

2.1. Study area

This case study was conducted in Bologna, a municipality in the Emilia-Romagna region of Italy, as represented in Fig. 1 along with a key map showing its location within Italy. Bologna is a densely populated city in the region and has a significant demographic ratio. It is characterized by a diverse urban morphology, with a mixture of historical architecture, densely built environments, and green spaces. Dense, compact buildings mark the city's central urban core, while its peripheral areas transition into a mix of residential, industrial, and agricultural landscapes. Bologna lies within a humid subtropical - Mediterranean transitional climate regime, exhibiting marked seasonal thermal variability typical of northern Italian lowland environments. This heterogeneity in land use, combined with significant seasonal temperature variations, made it an ideal location for studying the neighborhood-scale dynamics of urban thermal environments. Moreover, it has experienced significant urbanization and economic growth, posing challenges related to urban heat and thermal comfort, especially during summer when heat waves have been recorded more frequently in Europe. The presence of mixed land cover types, ranging from densely populated urban areas to agricultural fields and forested regions in the surrounding hills, made it a microcosm for understanding the spatial scale effects of urban heat in both central and peripheral areas. This diversity enhanced the ability to draw broader insights into the relationship between urban morphology, human activities, and thermal stress across different landscapes and seasons.

2.2. Datasets used

To predict the super-resolved surface temperature, this study utilized the Landsat-derived LST and land use indices derived from Landsat and Sentinel, by following the approach used in previous studies for downscaling LST using Sentinel and Landsat datasets (Rao et al., 2024a, 2025). In addition, Morphological Settlement Zones (MSZs) was used to consider the detailed urban morphology of the study area. MSZ, as defined by the Global Human Settlement Layer (GHSL), provides a detailed classification of human settlements based on their physical structure and density. These zones categorize land use into urban, peri-urban, and rural areas, based on the continuity and concentration of built-up areas. MSZs had been instrumental in understanding how different settlement patterns impact environmental factors, including LST.

Moreover, Urban Atlas, provided by the Copernicus Land Monitoring Services (CLMS), offered high-resolution land use and land cover

Table 1
Datasets used, (GEE: Google Earth Engine; CLMS: Copernicus Land Monitoring Services; GHSL: Global Human Settlement Layer; ESA: European Space Agency.

Data	Source/Platform	Year	Resolution
LST (Satellite Derived)	Landsat/GEE	2021	30 m
LST Downscaled	Landsat+Sentinel/GEE	2021	10 m
Urban Atlas	CLMS (https://land.cpernicus.eu/en/products/urban-atlas)	2018	100 m
MSZ	GHSL (https://human-settlement.emergency.copernicus.eu/download.php?ds=builtC)	2018	10 m
Built-up surface	GHSL (https://human-settlement.emergency.copernicus.eu/download.php?ds=bu)	2018	10 m
Tree Cover	ESA World Cover/GEE (https://developers.google.com/earth-engine/datasets/catalog/ESA_WorldCover_v100)	2020	10 m
Population Density	GHSL (https://human-settlement.emergency.copernicus.eu/download.php?ds=pop)	2020	100 m

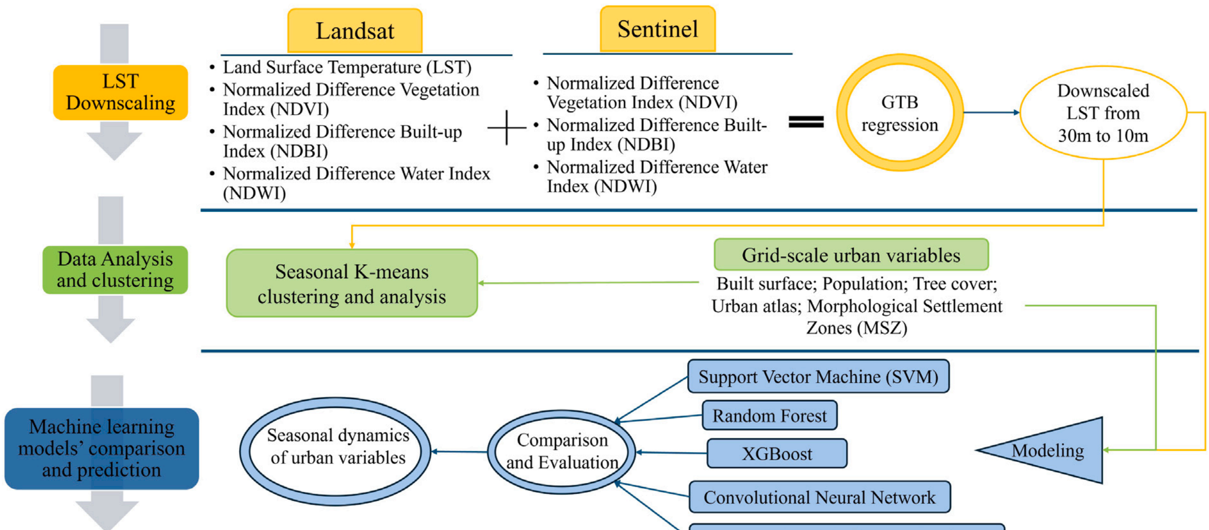

Fig. 2. Method flow describing the steps of LST downscaling, followed by data analysis and clustering of the grids based in urban variables, and finally the quantification of seasonal dynamics using multiple machine learning models.

data specifically designed for urban areas across Europe. In this study, it was selected to ensure future extendibility to other European cities. It provided detailed urban feature classifications, including residential zones, green spaces, industrial areas, and transportation networks. Mapping these elements resulted in a comprehensive overview of how land had been utilized within cities. Furthermore, built-up surface distribution, in addition to population density provided by GHSL datasets, was used along with high-resolution tree cover provided by CLMS to quantitatively assess the proportion of land use under pervious and impervious types, along with the anthropogenic activity load. Although these datasets originate from varying years (but close to LST year), this temporal mismatch is acceptable for the present analysis. Urban morphology and land-use patterns at the neighborhood scale are quasi-static over short periods, and the other datasets were selected based on the closest availability to the LST year. The 2021 LST was chosen as it represents a recent extreme-heat reference year, relevant for examining urban thermal dynamics. The dataset details have been described in Table 1.

2.3. Methodology

All datasets used in this study were first downloaded, processed, and harmonized according to the sources listed in Table 1. LST was initially estimated at 30 m resolution using Landsat data and subsequently downscaled to 10 m using Sentinel-2 spectral indices. The methodological workflow (Fig. 2) outlines the complete pipeline, including data acquisition, LST downscaling, clustering, and predictive modeling.

2.3.1. LST prediction at a high spatial resolution

Landsat-derived LST (30 m) was computed using the Landsat Collection 2 Level-2 product (LANDSAT/LC09/C02/T1-L2) processed within Google Earth Engine. Cloud and cloud-shadow pixels were masked using QA-PIXEL bitmask filtering prior to analysis. This Landsat LST served as the foundation for analyzing thermal conditions but lacked the spatial detail required for neighborhood-scale assessment. To obtain finer thermal patterns, LST was downscaled using Sentinel data and corresponding land-use spectral indices. Landsat LST was regressed against land-use indices, namely, normalized difference vegetation index (NDVI), normalized difference built-up index (NDBI), and normalized difference water index (NDWI), all at 30m resolution, using a Gradient Tree Boost (GTB) model. The detailed workflow of the downscaling approach can be referred to previous studies (Rao et al., 2024a, 2025), where the results indicated good agreement, with correlation coefficient > 0.70 and reaching upto 0.85 in a representative case, and high coefficient of determination (R^2) ranging from 0.61 to 0.72, with $p < 0.001$. After model calibration using an 80/20 train–test split and satisfactory validation accuracy, Sentinel-derived indices at 10 m resolution replaced the Landsat predictors to generate downscaled LST for 2021, one of the warmest years of the decade. The regression relationships were calibrated and validated separately for each season at Landsat resolution prior to application at finer scale. Because the predictors are normalized spectral indices representing consistent biophysical properties, the learned relationships are expected to remain transferable across sensors. The predictors (land-use variables) were derived from optical imagery of Sentinel-2 Level-2A surface reflectance data (COPERNICUS/S2-SR), filtered for scenes with less than 20% cloud cover and masked using QA60-based cloud and cirrus screening. Seasonal composites were constructed using all scenes with less than 20% cloud cover, grouped into winter (December to February), spring (March to May), summer (June to August), and autumn (September to November). Median LST values were computed for each season using reduction functions in Google Earth Engine. Due to limited availability of temporally coincident Landsat and Sentinel acquisitions across all seasons, seasonal median compositing was adopted to minimize sampling bias and suppress scene-specific variability. This strategy ensured robust representation of seasonal thermal conditions prior to predictor substitution with Sentinel-derived indices for downscaling.

2.3.2. Clustering of urban grids

Cluster analysis is used to identify and separate groups within a dataset by examining the similarities and differences between the individual elements. Elements that share common features are grouped together, while those with distinct characteristics are placed into separate clusters. It is a multi-step process that requires careful consideration at several stages. Three key decisions must be made: first, identifying and preparing the appropriate data for analysis; second, selecting a suitable method for measuring similarity or distance between data points; and third, choosing the most suitable clustering algorithm to effectively group the data.

To identify distinct neighborhood-scale thermal regimes, seasonal LST values were extracted within a 200 × 200 m grid framework. Unsupervised clustering was then performed to group grid cells with similar thermal and biophysical characteristics separately for each season to capture season-specific spatial thermal structures rather than imposing a unified clustering. The analysis included approximately 3500 valid grid cells per season, providing the sample basis for evaluating cluster compactness and separation. Four continuous variables: tree cover, population density, built surface, and seasonal temperature, were selected as core descriptors of urban form and microclimate. Before clustering, variables were standardized using z-score normalization. Principal Component Analysis (PCA) was applied to enhance computational efficiency and reduce redundancy. K-means clustering (scikit-learn) was implemented, and the optimal number of clusters was determined through the Elbow Method and Silhouette Score. The elbow and silhouette diagnostics consistently supported a four-cluster solution across seasons. Cluster validity was further evaluated using Calinski-Harabasz and Davies–Bouldin indices. The first two PCA components retained approximately 78%–80% of feature variance, and validation scores indicated well-separated structures (Calinski–Harabasz range: 3923–5173; Davies–Bouldin range: 0.74–0.79). Spatial patterns were visualized in PCA space, and cluster-wise variable distributions were assessed using boxplots and stacked bar charts integrating categorical land-use and morphology layers.

To evaluate the influence of seasonal LST on cluster formation, additional clustering analyses were performed using only built tree cover, population density, and built surface. The resulting cluster assignments were compared with the corresponding seasonal clustering solutions that included LST using the Adjusted Rand Index (ARI). This index ranges from 0.0 to 1.0, where 0.0 indicates no agreement beyond random and 1.0 indicates identical clustering. ARI values were calculated separately for spring, summer, autumn, and winter to quantify the degree of agreement between morphology-based and thermal-morphology-based clustering solutions.

2.3.3. Machine learning modeling and explainable interpretability framework

Following the identification of neighborhood-scale thermal patterns, machine learning and deep learning models were employed to quantify the seasonal influence of morphological, environmental, and socio-economic variables on LST. Four benchmark algorithms, namely, Support Vector Machine (SVM), Random Forest (RF), XGBoost, and a 1-D Convolutional Neural Network (1D-CNN), were implemented to capture varying degrees of linear and nonlinear relationships among predictors.

The dataset was randomly split into 90% training and 10% testing subsets. Categorical variables (Urban Atlas and UMZ) were incorporated into the model using ordinal encoding, whereby each class was assigned a unique numerical identifier. These numbers are inherently nominal rather than ordinal. This approach was adopted to provide a compact representation of categorical information for model training. Subsequently, they were normalized using MinMax scaling and the models were trained using fixed parameter settings. SVM models complex feature relationships in high-dimensional space through kernel transformations. RF provides ensemble-based robustness against overfitting while enabling inspection of hierarchical decision patterns. XGBoost, a gradient boosting framework, enables efficient learning by minimizing the loss function through additive tree modeling. Deep learning was represented using a 1D-CNN, which learns localized feature dependencies through convolutional operations (LeCun et al., 2015; Singh and Bruzzone, 2022). In particular, deep learning-based models are successful in modeling information by fusing complex features (Singh and Bruzzone, 2025).

Finally, a transformer-based convolutional regressor, shown in Fig. 3, was designed to enhance feature sensitivity analysis. The input sequence was defined as $X = x_1, x_2, \ldots, x_n$, where each x_i represented a feature. In order to extract the complex relationship between the features, we designed the task-specific transformer-enabled convolutional regressor, which consists of a convolutional operation followed by a transformer layer. The output of the convolutional operation can be represented as:

$$C(X_l) = \varphi\left(\sum_{m=1}^{p} F_m * X_{l,m} + b\right) \quad (1)$$

In Eq. (1), ϕ is the activation function, in which k is the kernel size and F is the number of filters for p features per sample, F_m is the convolution filter applied to the feature m, $*$ denotes the convolution operation and b represents the bias term. After the convolution operation $C(X_l)$, followed by a transformer block consists of layer normalization, multi-head attention, followed by a Multi-Layer Perceptron (MLP). It helped the model to selectively focus on the sensitive features while making predictions. For the training of the model, the Adam (Adaptive Moment Estimation) was used with a learning rate of 0.001, and the kernel size was set to 2. During the experimental training, the batch size was set to 32, and the number of epochs was set to 100. In the proposed formulation, the tabular predictors are treated as a structured sequence of heterogeneous inputs (Singh et al., 2025). The CNN component provides an efficient mechanism for extracting local feature interactions and compact representations, while the transformer block captures global, long range dependencies across all predictors. Importantly, the transformer's attention mechanism evaluates relationships between features, independent of their position in the sequence.

To ensure interpretability of the predictive framework, Explainable AI (XAI) techniques, illustrated in Fig. 4, were incorporated directly into the modeling workflow to interpret model behavior and derive transparent insights into LST drivers. Feature importance is examined with respect to LST using the proposed approach which involves all the input features. The attention properties of the transformer block are used only as a additional component to understand how the model captures long range dependencies and distributes focus during learning. Because the model includes multiple convolutional and transformer stages that progressively transform the feature representations (4,64)→(3,32)→(2,16)→(1,16), the resulting sensitivity analysis reflects the combined effect of all components..

The results from each model were compared to understand how factors like population density, MSZ, urban atlas classes, built surface, and tree cover area influence the urban thermal environment. Further, the best-performing model was subsequently used to predict the relative influence of all selected urban parameters on the seasonal thermal patterns.

3. Results

3.1. Super-resolved Land Surface Temperature (LST)

The GTB regression approach was used to improve the spatial resolution of the Landsat-derived LST grids from their native resolution to

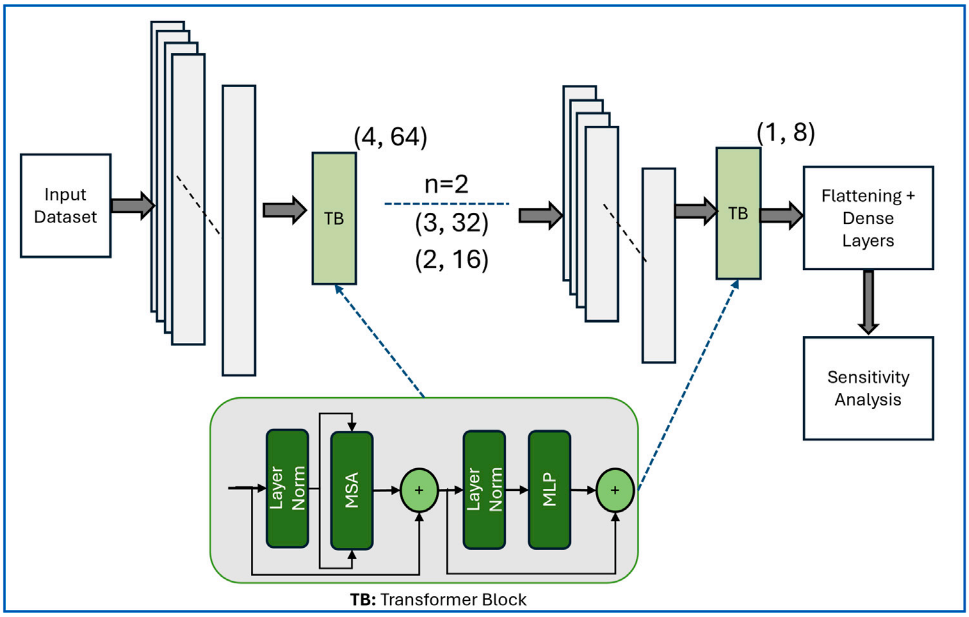

Fig. 3. Proposed transformer based convolutional approach for the sensitivity analysis.

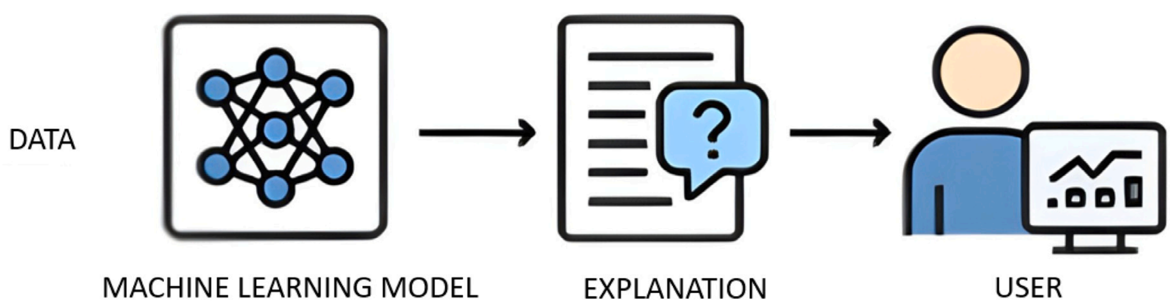

Fig. 4. Illustration of Explainable AI (XAI).

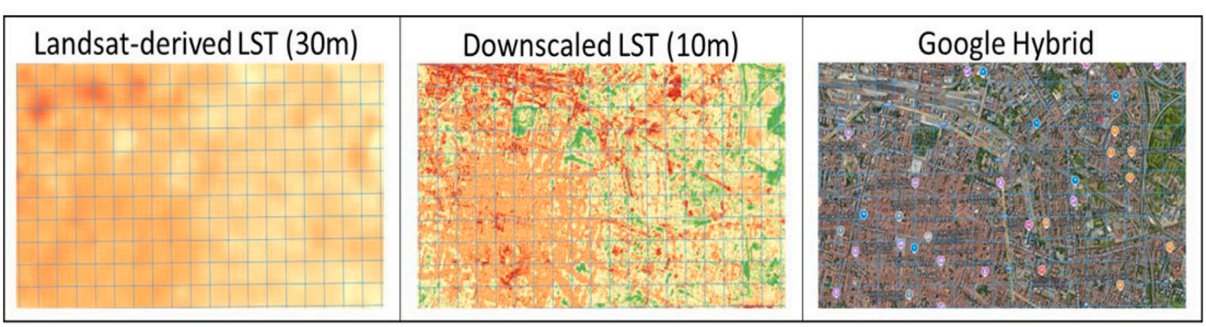

Fig. 5. Landsat-derived LST v/s Sentinel-based downscaled LST.

10 m, using NDVI, NDBI and NDWI as predictive variables. Fig. 5 shows the resulting super-resolved LST map, which demonstrates significantly finer thermal detail compared to the original Landsat product.

The predictive performance of the GTB model for downscaling LST was validated against the corresponding Landsat LST for an independent summer-day image within the study year. The validation showed a significant positive relationship between predicted and Landsat LST (R = 0.73, R^2 = 0.53, p<0.05). The model produced a small negative bias (Mean Bias Error = −0.38 °C), indicating a slight tendency to underestimate LST while preserving the overall spatial variability. Seasonal prediction errors remained relatively low, with mean errors of 0.45 °C in spring, 0.32 °C in summer, 1.41 °C in autumn, and 0.72 °C in winter. These results suggest that the GTB model provides reasonably consistent LST predictions across seasons, with some variations in the prediction accuracy. It should be noted that, although similar validation approaches have been adopted in other LST downscaling studies when independent reference data are unavailable, the present validation is not fully independent and therefore remains a source of uncertainty. Errors and biases inherent in the Landsat-derived LST may propagate into the downscaled product. Consequently, the reported validation statistics should be interpreted as an indication of the model's ability to preserve spatial thermal patterns and seasonal variability rather

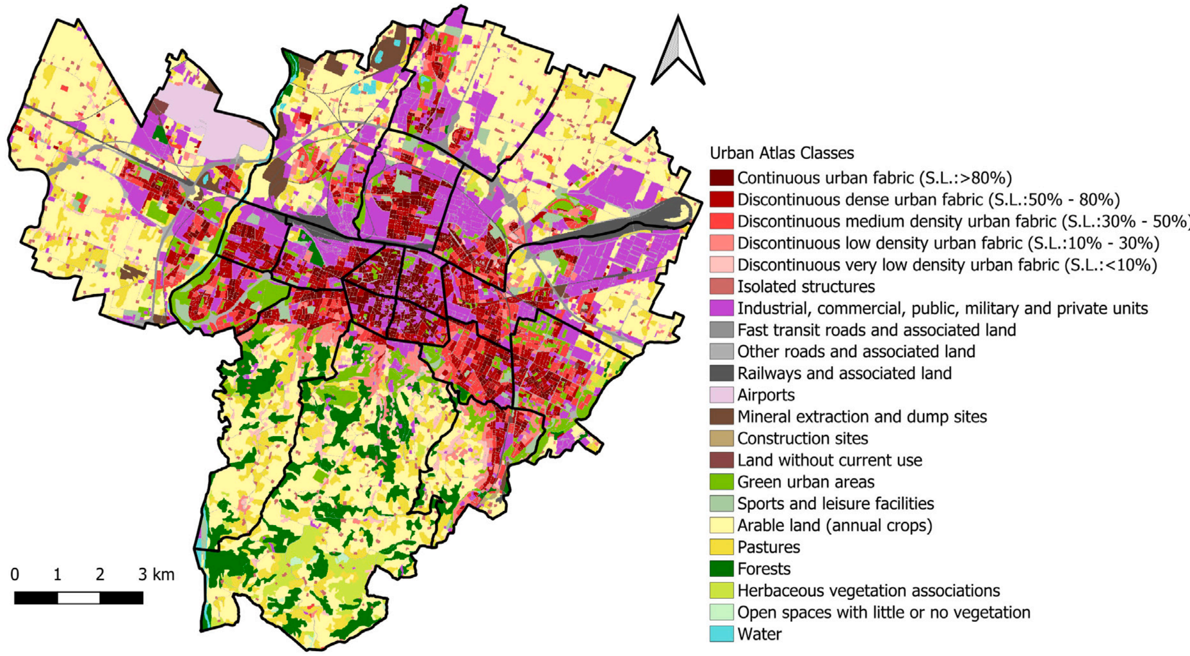

Fig. 6. Spatial distribution of the urban atlas classes, provided by the Copernicus Land Monitoring Services (CLMS) at 100 m spatial resolution.

than as a direct measure of absolute fine-scale temperature accuracy. Accordingly, the results derived from the downscaled LST should be interpreted with this limitation in mind.

3.2. Distribution of urban variables

Urban atlas classes provide a standardized classification of land use and land cover across European urban areas, offering a functional overview of urban landscapes. In this study, the 2018 Urban Atlas layer, sourced from the Copernicus Land Monitoring Service, was used to delineate broad land use categories and their spatial distribution within the study area (Fig. 6). Pervious land cover types, particularly arable land (annual crops), dominate the outer regions of the city and occupy the largest number of spatial grids. This reflects the persistence of agricultural activity around the urban periphery. Among impervious surfaces, industrial, commercial, public, military, and private units, along with continuous urban fabric, are the most prevalent classes. These are primarily concentrated in the urban core and industrial zones, aligning with areas of high development density. While the Urban Atlas provides essential baseline information on land use functionality, its classification does not explicitly account for structural attributes such as building height or vegetation density. Nonetheless, it serves as a critical contextual layer for interpreting surface temperature variations across different land use zones in the urban environment.

Urban morphological settlement zones (MSZ) provide a detailed characterization of urban form by integrating land use, vegetation cover, and vertical built-up structure. It enhances the spatial resolution of urban morphology and allows for a more detailed investigation of how variations in building type, density, and vegetation contribute to urban microclimates. The classification framework follows a hierarchical scheme, beginning with the distinction between built-up and open spaces, and further subdividing them based on surface characteristics such as NDVI ranges (for open spaces) or building height ranges (for built-up areas). This enables a subtle understanding of the spatial heterogeneity of urban structure. As shown in Fig. 7a, the dominant MSZ class in the study area is Class 13, representing residential built-up zones with building heights ranging from 6 to 15 m. This class occupies the largest number of spatial grids, primarily located within medium-density residential neighborhoods.

The second most prevalent category is Class 3, defined as open spaces with high vegetation density (NDVI>0.5), which are distributed mainly in peripheral zones and green corridors within the urban matrix. Class 23, corresponding to non-residential built-up areas with similar building height ranges (6–15 m), also shows a significant presence, particularly in commercial and institutional zones. The MSZ classification enhances the spatial resolution of urban morphology and allows for a more detailed investigation of how variations in building type, density, and vegetation contribute to urban microclimates.

Urban tree cover represents the proportion of land area within each grid that is occupied by tree canopies, providing a direct indicator of vegetative presence in the built environment. Fig. 7b displays the spatial distribution of tree cover across the study area at a 10 m resolution. The data were aggregated to the analytical grid scale for quantitative assessment. The resulting values indicate that tree cover varies between 0% and 20% across the grids, with most areas showing relatively sparse vegetation. Spatially, higher concentrations of tree cover are observed in green corridors, peripheral zones, and certain residential neighborhoods, whereas central urban and industrial areas exhibit minimal tree presence.

Built surface fraction quantifies the proportion of each grid area that is covered by impervious built-up surfaces, such as buildings, roads, and paved infrastructure. As shown in Fig. 7c, the spatial distribution of built-up fraction was mapped at a 10 m resolution and subsequently aggregated to the grid scale for analysis. The results reveal a variation in built surface coverage from 0% to 20%, reflecting a spatially heterogeneous urban fabric. Denser built-up fractions are concentrated in the central parts of the Bologna commune, while lower values are observed in peripheral and open space areas.

Urban population density reflects the distribution of inhabitants across the study area and is a key socio-demographic variable that influences urban microclimates in the form of anthropogenic heat. Fig. 7d illustrates the spatial variation in population density using data obtained from the Global Human Settlement Layer (GHSL) at a native resolution of 100 m, later resampled to the analytical grid scale for consistency. To facilitate quantitative interpretation, population

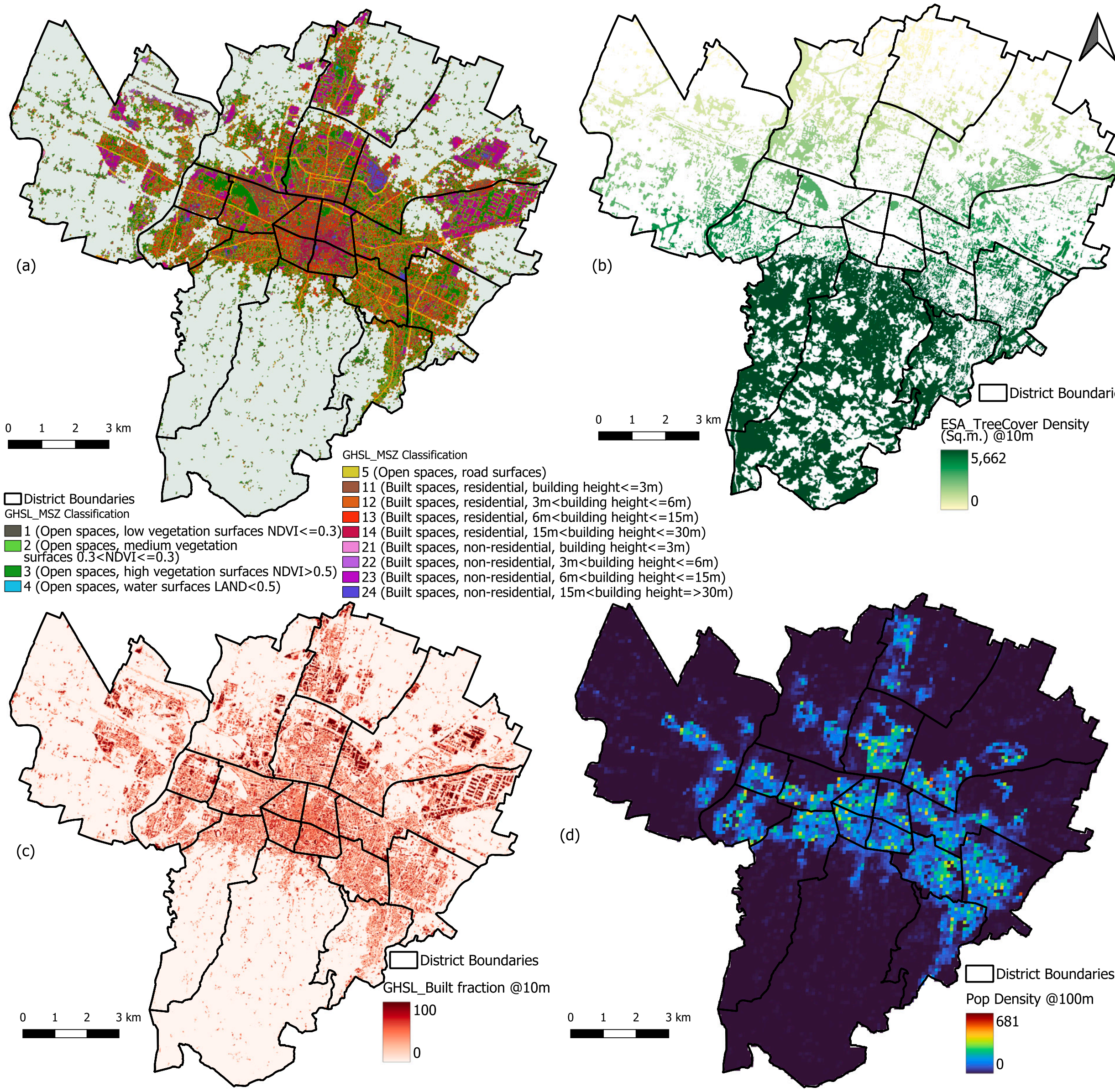

Fig. 7. Spatial distribution of the urban parameters, where (a) urban morphological settlement zones (MSZ); (b) urban tree cover, provided by the European Space Agency (ESA) at 10 m spatial resolution; (c) GHSL's built fraction at 10 m spatial resolution; (d) population density at 100 m spatial resolution, provided by the GHSL.

values were classified into five equal-interval categories: very low, low, medium, high, and very high. The classification shows that most grids fall under the very low category (<364.90 persons per grid), with progressively fewer grids in higher density classes. Spatially, higher density zones are located near urban centers and key residential clusters, while peripheral and transitional zones exhibit lower population concentrations. It is to be noted that these variables reflect the proportion of each 200 × 200 m grid cell occupied by the respective land cover, aggregated from higher-resolution datasets. Therefore, even in the dense urban core, grid cells include roads, courtyards, and open spaces, which limits the maximum built fraction to values below 100%. Minor reductions may also arise from masking and aggregation artifacts. This representation provides a consistent basis for analyzing spatial variations in LST across heterogeneous urban neighborhoods.

These five urban parameters were identified as key influencing factors on seasonal LST. Analyzing the Urban Atlas and MSZ as separate variables enables a comprehensive assessment of functional land use information, incorporating detailed morphological characteristics of urban form. While the MSZ captures the structural aspects of settlements, including building heights, spatial layout, and density, the Urban Atlas focuses on functional classifications such as residential, industrial, and agricultural land uses. These categorical variables provide complementary perspectives on urbanization patterns and their thermal implications. To ensure that their joint inclusion does not introduce redundancy, the association between the two classification schemes was quantified using Cramér's V, yielding a value of 0.35, indicative of moderate correspondence rather than collinearity. This confirms that each dataset represents distinct dimensions of urban structure. Additional multicollinearity diagnostics using variance inflation factor (VIF) analysis yielded values ranging from 2.5 to 7.9 (population: 2.5; tree cover: 3.32; builtup surface: 4.66; urban atlas-sin: 3.24; urban atlas-cos: 3.22; MSZ-sin: 7.46; MSZ-cos: 7.89). While most predictors exhibited low-to-moderate multicollinearity, relatively higher VIF values were observed for the transformed Urban Atlas and MSZ encoding components, partly reflecting dependency introduced by the sine–cosine representation. However, none of the predictors

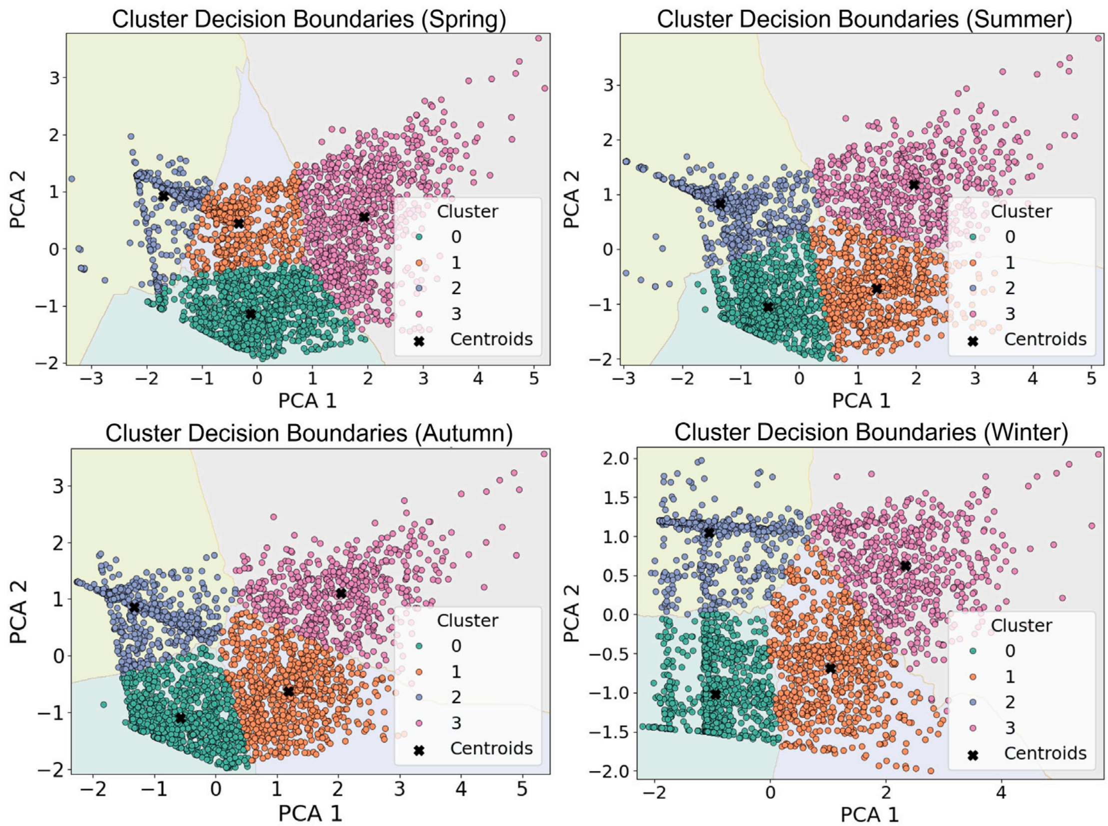

Fig. 8. Cluster Decision Boundaries.

exceeded the commonly accepted critical threshold of VIF> 10 (O'brien, 2007), indicating the absence of severe multicollinearity. These results support the overall stability of the modeling framework while acknowledging moderate dependency among certain transformed predictors. In parallel, the continuous variables, built surface fraction, urban tree cover, and population density, further enrich the spatial understanding of thermal dynamics. Built surface fraction quantifies the extent of impervious surfaces, which are typically associated with elevated heat retention. Urban tree cover reflects the distribution of vegetative cooling potential. Population density serves as a proxy for anthropogenic pressure, representing the concentration of human activities and associated heat emissions that can elevate temperatures. Collectively, these parameters provide critical spatial context for evaluating urban thermal conditions and informing targeted mitigation strategies.

3.3. K-means clustering of urban surface characteristics across seasons

To explore the spatial patterns of urban surface characteristics and their seasonal variability, a K-means clustering algorithm was applied to four normalized continuous variables, excluding categorical datasets such as the Urban Atlas and MSZ. Dimensionality reduction was performed using PCA, and the resulting two-dimensional feature space was used for visualization. Fig. 8 illustrates the spatial distribution of cluster memberships and the corresponding decision boundaries across all four seasons. In addition, the influence of seasonal LST on cluster formation was evaluated using the ARI. The comparison between clustering solutions generated with and without LST produced ARI values of 0.574, 0.738, 0.705, and 0.760 for spring, summer, autumn, and winter, respectively. These results indicate moderate to strong agreement across all seasons, demonstrating that the inclusion of seasonal LST did not fundamentally alter the underlying cluster structure. Instead, seasonal LST refined cluster boundaries by incorporating season-specific thermal information while preserving the primary patterns associated with built surface fraction, tree cover percentage, and population density. The lower ARI observed in spring suggests that seasonal temperature patterns exert a comparatively stronger influence on cluster differentiation during this transitional period. Spring is characterized by rapidly changing vegetation conditions, surface moisture, and atmospheric processes, which may increase spatial variability in thermal responses. Nevertheless, the ARI value remained substantially above zero, indicating that the morphology-based cluster structure was still largely preserved. The results reveal distinct seasonal shifts in the organization of urban clusters, indicating that the surface characteristics exhibit dynamic behavior throughout the year. Each subplot highlights how clusters reorganize spatially between seasons, reflecting variations in the thermal and physical properties of the urban landscape. This seasonal clustering approach provides an interpretable framework for understanding how different combinations of urban features influence surface variability over time.

3.3.1. Spatiotemporal dynamics of urban clusters across seasons

The grids were classified into four distinct spatial clusters for each season, based on a combination of static land cover, socioeconomic characteristics, and seasonally varying LST. Fig. 9(a) demonstrates the seasonal spatial distribution of these clusters across the study area. Despite seasonal variations, the clusters maintained a thematic consistency with Cluster 0 being characterized by low built-up density and high agricultural land cover, typically located in peri-urban and rural zones; Cluster 1 represented mixed zones with combination of industrial, residential, and agricultural land uses; Cluster 2 dominated by high tree cover, and low built-up density; and Cluster 3 majorly comprised of the urban core, with high impervious surface coverage, and sparse vegetation. Spatially, a stable core–periphery structure was observed across all seasons. Cluster 3 remained concentrated in central

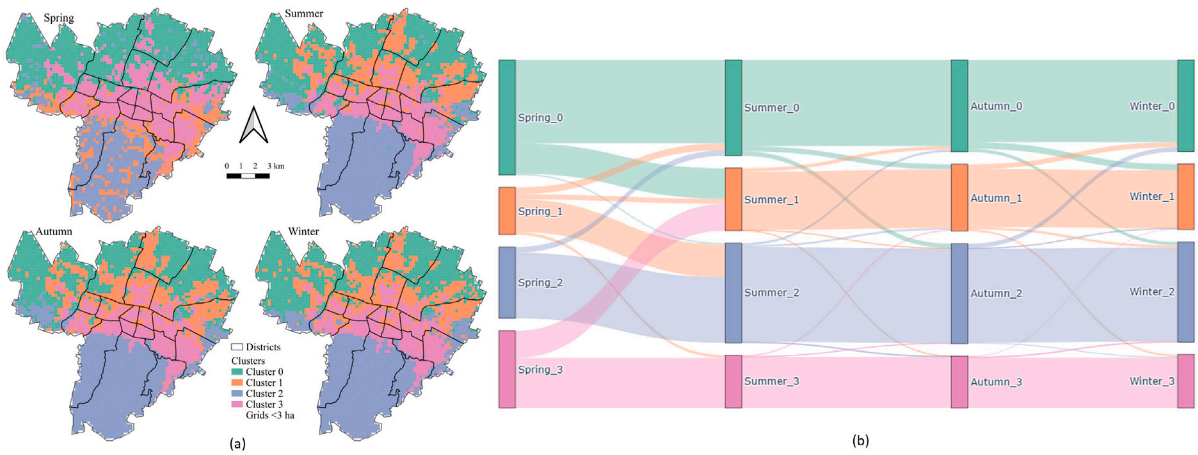

Fig. 9. Seasonal clusters: (a) Spatial distribution; (b) Seasonal cluster transition Sankey diagram.

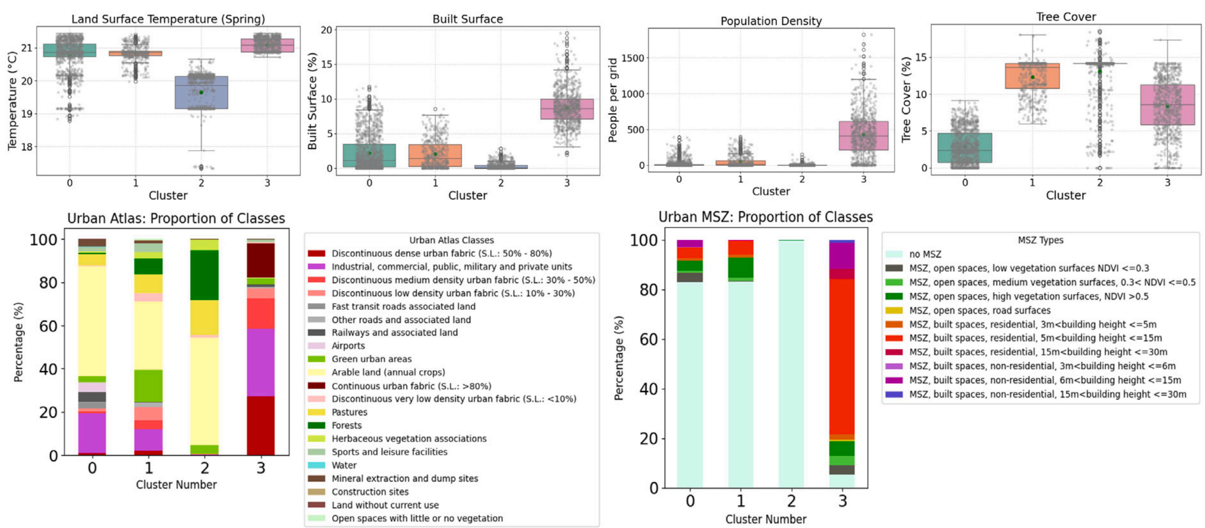

Fig. 10. Quantitative distribution of continuous and categorical variables across clusters for the Spring season.

Bologna, reinforcing its role as a persistent thermal hotspot with minimal seasonal spatial change. Cluster 2, associated with vegetated zones, also demonstrated strong spatial stability. In contrast, Clusters 0 and 1 exhibited greater variability across seasons.

These intra-annual dynamics are further illustrated in the Sankey diagram (Fig. 9(b)), where each node represents the grid assignments in a specific cluster and season, while the connecting flows indicate transitions between clusters over time. While many grids retained their cluster identity across all four seasons, particularly in Clusters 2 and 3, Cluster 1 displayed pronounced transitions. Most Cluster 1 grids in spring transitioned into Cluster 2 during summer, while the composition of Cluster 1 in summer originated almost equally from spring Cluster 0 and Cluster 3. This confirms that Clusters 0 and 1 represent the most fluid categories, with frequent reclassification compared to the more stable behavior of Clusters 2 and 3. These transitions may have taken place probably due to seasonal modulations in surface thermal characteristics and land surface processes driven by both biophysical and human-induced factors. It is to be noted that the transitions illustrated in the Sankey diagram were quantitatively verified using transition counts and proportional summaries, confirming consistency between the graphical representation and the underlying cluster redistribution patterns. The diagram is therefore retained as the primary means of communicating seasonal transition dynamics.

3.3.2. *Statistical comparison of cluster characteristics across seasons*

The quantitative distribution of continuous variables and the composition of categorical land classes across clusters demonstrated clear and seasonally consistent patterns. Figs. 10 to 13 present box plots with overlaid scatter points depicting the variability of continuous variables across the four clusters in each season, accompanied by stacked bar plots showing the relative composition of land-use (Urban Atlas classes) and urban morphological types (MSZ).

Across all seasons i.e., Spring (Fig. 10), Summer (Fig. 11), Autumn (Fig. 12), and Winter (Fig. 13), as expected from the inclusion of seasonal LST in the clustering variables, Cluster 3 consistently exhibited the highest seasonal LST; importantly, this cluster was also characterized by the highest built-surface proportion and population density, indicating a persistent association between thermal intensity and compact urban morphology. Cluster 2 exhibited the lowest LST and the highest vegetation cover, minimal built surfaces, and low population density, encompassing forests, arable lands, and meadow areas. Cluster 0 remained dominated by agricultural and industrial land uses, with moderate LST values, low tree cover, and sparse population, while Cluster 1 comprised a heterogeneous mix of urban and non-urban features, exhibiting intermediate conditions. Seasonal variations were mainly evident in the magnitude of LST differences among clusters, with greater contrasts during spring and summer, and reduced variability

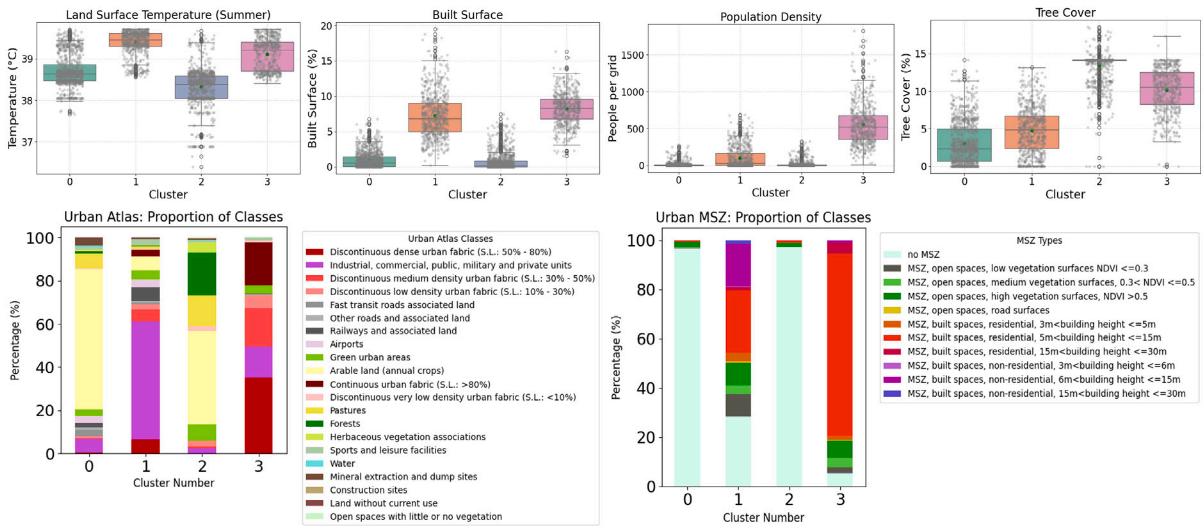

Fig. 11. Quantitative distribution of continuous and categorical variables across clusters for the Summer season.

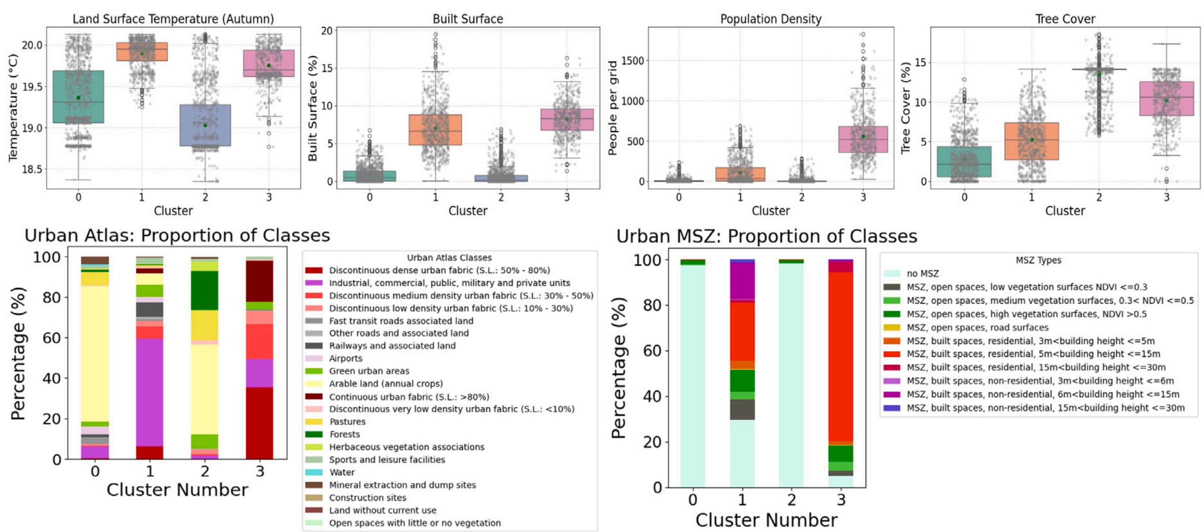

Fig. 12. Quantitative distribution of continuous and categorical variables across clusters for the Autumn season.

in autumn and winter. The distribution of land-use and morphological types remained largely stable across all seasons, indicating a persistent spatial configuration of the identified clusters.

3.4. Comparative analysis of seasonal variable influence on LST

3.4.1. Model performance evaluation

To quantify the seasonal influence of urban morphological and socioeconomic factors on LST, a comparative assessment of five predictive modeling techniques: Support Vector Machine (SVM), Random Forest (RF), XG Boost, general CNN (convolutional neural network), and the proposed model (CNN + Attention) was performed. The models' performance was evaluated using standard validation metrics (error based performance matrix), including the coefficient of determination (R_2), root mean square error (RMSE), and mean square error (MAE), as summarized in Table 2. Paired statistical tests (paired t-test and Wilcoxon signed-rank) were applied as complementary diagnostics using a standard significance level, and broadly supported the observed performance trends across seasons, while reflecting expected variability associated with environmental heterogeneity. Among the tested models, the proposed model achieved comparatively better performance, with the highest R^2 value (0.57) and the lowest RMSE (0.10), indicating improved accuracy in LST estimation. While both the proposed model and XGBoost attained similar R^2 values, the proposed CNN exhibits consistently lower RMSE and MAE, indicating improved prediction accuracy at the neighborhood scale. Repeated model runs confirm the robustness of these error-based performance improvements, demonstrating that error-based metrics provide a more sensitive assessment of fine-scale LST variability than R^2 alone. Moreover, the proposed model more effectively captured the joint influence of multiple predictors (Table 3), whereas, XGBoost disproportionately emphasizes a single variable (built surface: 68.9%), underrepresenting others and reflecting its sensitivity to dominant features. These results highlight the constructed model's ability to deal with nonlinear and complex interactions among multiple predictor variables driving thermal variability.

3.4.2. Seasonal influence of urban on temperature

To identify the key drivers of LST across seasons, the best-performing model was employed to quantify the relative influence of urban morphological and socioeconomic variables. The analysis demonstrated a seasonally varied pattern of variable importance, reflecting the dynamic and multifactorial nature of urban thermal behavior. Across all seasons, built surface consistently emerged as the most influential predictor, contributing between 37.7% and 41.4% to LST estimation.

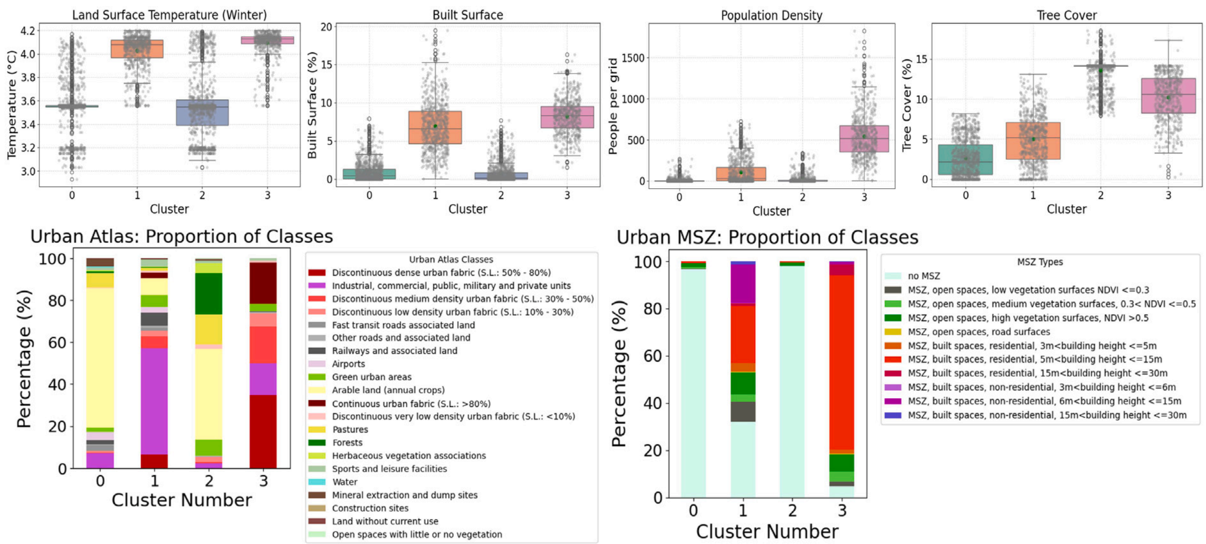

Fig. 13. Quantitative distribution of continuous and categorical variables across clusters for the Winter season.

Table 2
Performance statistics of different models used to predict LST.

Model	R-squared	RMSE	MAE
Support Vector Machine (SVM)	0.50	0.11	0.08
Random Forest (RF)	0.54	0.11	0.08
XG Boost	**0.57**	**0.11**	0.08
Convolutional Neural Network (CNN)	0.53	0.11	0.08
Proposed model (CNN+Transformer)	**0.57**	**0.10**	0.08

Table 3
XG Boost and proposed method-derived variable importance on LST for the summer season.

Variable	XG Boost	Proposed method
Built Surface	68.9%	37.7%
Urban Atlas	5.6%	18.5%
Tree Cover	14.8%	11.5%
MSZ	7.6%	12.7%
Population	3.1%	19.6%

Its dominance was most pronounced in winter (41.4%) and autumn (39.7%), and slightly lower in spring (38.8%) and summer (37.7%), reflecting the persistent thermal impact of impervious surfaces throughout the year. Population density displayed strong seasonal variability: while its influence was minimal in spring (5.5%), it increased substantially in summer (19.6%) and autumn (15.6%), reaching its contribution in winter (35.0%). This seasonal pattern may indicate broader associations between densely populated urban areas and seasonal variations in anthropogenic activity or energy use; however, these interpretations should be considered hypothesis-driven, as no direct proxies for energy consumption, traffic intensity, or mobility patterns were included in the modeling framework. Urban land-use classes also showed marked fluctuations, with relatively minor roles in spring (8.2%) and winter (8.6%), but substantially higher contributions in summer (18.5%) and autumn (20.3%), suggesting that functional land-use differences may become more relevant under warmer conditions. Tree cover contributed moderately in spring (9.6%) and summer (11.5%), consistent with its role in surface cooling, but its influence declined in autumn (11.2%) and further in winter (6.8%) as vegetation became less active. MSZ demonstrated high importance in spring (37.9%), comparable to built surface, but its contribution declined in summer (12.7%), autumn (13.1%), and winter (8.1%), indicating that built form and settlement configuration may have a more pronounced effect during transitional seasons. Collectively, these results highlight the influences of built surface while pointing to seasonally variable contributions of population, urban land-use classes, tree cover, and MSZ to LST variability. These patterns are illustrated in Fig. 14, showing the percentage contributions of each variable by season.

4. Discussions

4.1. Seasonal thermal structuring of urban environments

The seasonal clustering of urban characteristics revealed distinct and recurring spatial thermal patterns, highlighting the dynamic nature of surface temperature across the city. The K-means clustering algorithm, applied to a set of normalized urban variables, identified four thermally and environmentally meaningful classes that shifted in spatial extent and composition across seasons. These clusters reflected not only variations in surface temperature but also encapsulate the combined effects of land-use patterns, vegetation density, and population distribution (Rao et al., 2024b, 2023).

The most prominent thermal core, typically corresponding to Cluster 3, remained aligned with dense built-up areas characterized by high impervious surfaces and limited vegetative cover. This aligns with well-established evidence that such environments consistently exhibit elevated surface temperatures due to higher heat storage and reduced evapotranspiration. Meanwhile, cooler clusters, such as Cluster 2, were composed of high vegetation areas, including forest and green urban spaces, confirming the strong cooling influence of vegetation through processes like evapotranspiration and surface shading (Bowler et al., 2010; Rao et al., 2025). Transitional clusters (Clusters 0 and

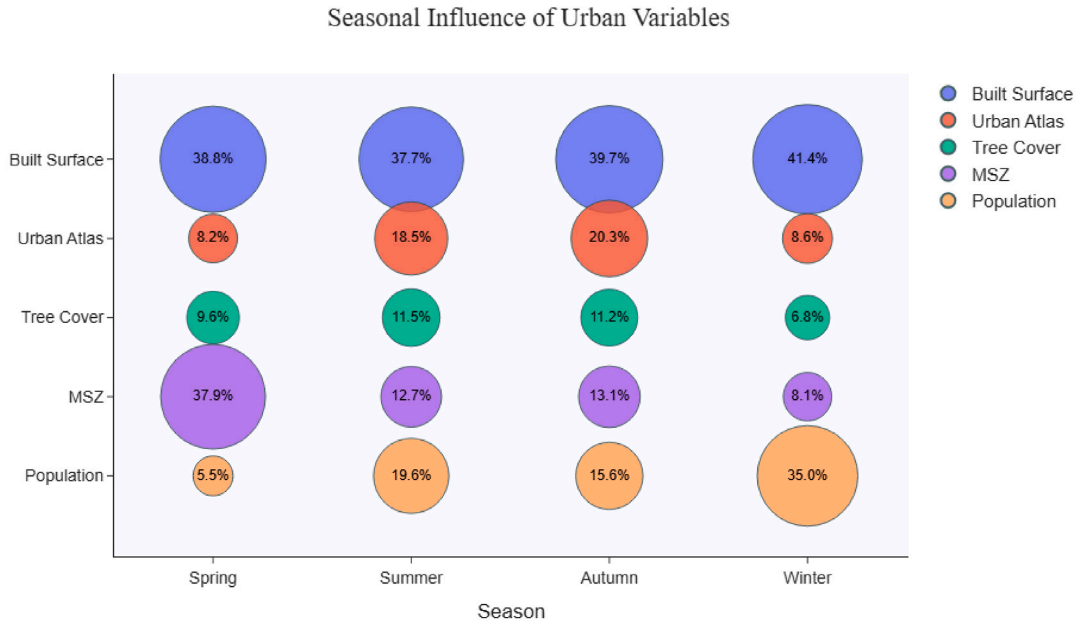

Fig. 14. Seasonal influential variation of urban factors over the thermal environment.

1) displayed marked seasonal variability, driven by vegetation cycles, agricultural activity, and local morphological changes (Lin et al., 2025). Their recurrent seasonal exchanges further illustrate the importance of capturing thermal patterns at high spatial resolution to uncover neighborhood-level microclimatic dynamics.

4.2. Structural composition of clusters and land use patterns

The comparison of land cover and morphological characteristics across clusters reaffirmed the strong link between urban form and seasonal thermal regimes. Cluster 3 consistently represented dense urban and industrial morphologies, with pronounced impervious fractions and vertical structures that enhance surface heating (Liang et al., 2024; Zhao et al., 2025). In contrast, Cluster 2 was dominated by vegetated classes, including forest areas and low-density built-up fabric with open green spaces, indicating their role in thermal mitigation. The stacked bar plots across seasons confirmed these land-use-based distinctions and emphasized the heterogeneity in land surface processes driving thermal variability (Rao et al., 2025, 2023). Clusters 0 and 1 displayed hybrid morphological compositions and distinct geographic expressions, underlining their dynamic thermal behavior (Talukdar et al., 2024).

Cluster 0 is predominantly associated with peri-urban and semi-rural mosaics in the northern plains, where agricultural land, fragmented built-up patches, and low tree cover produce unstable seasonal thermal responses (Q. Zhang et al., 2025), where seasonal growth and pasture drive marked shifts in surface temperature. Cluster 1 encompassed both agricultural plains and southern hilly areas with interspersed vegetation and built-up slopes. This duality made Cluster 1 highly sensitive to topographic factors, including slope orientation, solar exposure, and local wind regimes (Zou et al., 2025). Its seasonal transitions confirm this variability: in summer, many grids shift into Cluster 2 due to enhanced cooling from crops and vegetation at peak evapotranspiration, while overlap with Cluster 3 suggests that sparsely vegetated peri-urban built-up areas can thermally resemble urban fabric/built areas. Together, these patterns highlight that Clusters 0 and 1 represent hybrid and transitional zones, peri-urban, agricultural, and topographically modulated, that respond dynamically to seasonal land-surface processes. Unlike the clearer extremes of Clusters 2 and 3, they embody the challenge of characterizing edge and mixed environments, where fine-scale heterogeneity governs thermal variability (Y. Chen et al., 2022). Since seasonal LST was included as one of the clustering variables, thermal differentiation among clusters is partly reflected in the clustering outcome. However, comparison of clustering solutions generated with and without seasonal LST showed moderate to strong agreement across all seasons (ARI = 0.574–0.760), indicating that the overall cluster structure remained largely consistent. Therefore, the identified clusters should be interpreted as integrated urban thermal typologies in which seasonal temperature refines, rather than solely determines, the underlying patterns associated with built surface fraction, tree cover percentage, and population density.

Seasonal transitions, as captured through the Sankey diagram, illustrated the dynamic changes in grid cluster membership, underscoring the contrasting stability and variability across clusters. These patterns collectively further support the understanding that land cover composition, urban form, and vegetation interact to shape thermal environments, and that these interactions vary seasonally in both magnitude and spatial expression (Rao et al., 2024c,b, 2023; Song et al., 2025; Rao et al., 2024a). Cluster 1 showed substantial exchanges with vegetated classes in summer, while in other periods it converged with more urbanized thermal signatures. These patterns emphasize the importance of hybrid morphologies and geographic context (Rao et al., 2025) in shaping seasonal microclimates. This seasonal fluidity in thermal zones indicate that urban microclimates are responsive and adaptable, and underline the need for planning strategies that acknowledge such spatial complexity.

4.3. Seasonal influence of variables on LST

The deep learning-based variable contributions provided valuable insights into the drivers of urban thermal behavior. By resolving nonlinear relationships between predictors, the model was able to disentangle the unique role of each factor despite moderate inter-variable correlations. This distinction is particularly important because each variable captures different urban dynamics, for example, built surface reflecting impervious cover and heat retention, population density representing anthropogenic activity, and so on. Understanding these variations and the combined impact of certain variables is critical for identifying all possible key drivers of thermal patterns (Salvati et al., 2015), and for developing season-specific heat mitigation strategies.

Built Environment Effects (Built Surface and MSZ): Built Surface emerged as the consistently dominant contributor to urban surface temperatures (Han, 2023) across all seasons, highlighting the persistent thermal influence of impervious areas. The high heat storage capacity and low albedo of these surfaces, combined with limited evapotranspiration, allow them to retain and radiate heat year-round. For the urban MSZs, the influence was particularly pronounced in spring. During this transitional season, increasing solar radiation coincides with partial vegetation recovery, resulting in pronounced contrasts between dense, compact settlements and more open areas (Liu et al., 2024). These differences amplify local microclimatic variability, making MSZ one of the key drivers of surface temperature patterns in spring. In summer, the presence of fully developed vegetation and higher solar angles homogenizes thermal contrasts across settlement types, reducing the relative importance of MSZ. In autumn, although vegetation begins to senesce, the cooling effect of increasing rainfall and cloud cover moderate differences in thermal response between settlement types, further decreasing MSZ influence. During winter, low solar angles and the dominance of anthropogenic heating diminish the role of settlement morphology in shaping surface temperatures, as built form effects are overshadowed by uniform heat emissions and limited radiative gain. These seasonal variations highlight that while built surfaces maintain a persistent thermal effect, the relative contribution of settlement morphology is highly season-dependent, driven by interactions between solar geometry, vegetation dynamics, and local microclimatic contrasts (Marey et al., 2025).

Socio-Economic contributions (Population Density): Population density exhibited pronounced seasonal variability in its association with urban surface temperatures (Xu), ranging from minimal impact in spring to peak contribution in winter. This pattern may reflect broader seasonal differences in anthropogenic activity and energy demand commonly observed in densely populated urban environments (Antonopoulos et al., 2019); however, such interpretations remain hypothetical within the scope of the present study, since no direct indicators of energy consumption, traffic emissions, or human mobility were included in the analysis. Summer and autumn contributions, although lower than in winter, may similarly reflect indirect associations with increased urban intensity.

Tree Cover Effects: Tree cover played a major cooling role in spring and summer, driven by dense foliage, high transpiration rates, and greater solar exposure (Meili et al., 2021). In summer, vegetation continues to moderate heat, but its relative influence declines as higher baseline temperatures and anthropogenic emissions intensify the thermal load. This effect may be further exacerbated in non-irrigated public green areas, where drought stress reduces vegetation activity and limits evapotranspiration efficiency (Rao et al., 2025). During autumn, progressive leaf senescence decreases canopy density and transpiration rates, weakening the cooling potential of trees. In winter, most deciduous species are dormant, leading to minimal thermal regulation. These findings demonstrate the importance of maintaining and expanding tree canopy cover (Meili et al., 2021), particularly in seasons of peak heat.

Urban Land Use Effects (Urban Atlas Classes): Urban land use, as represented by Urban Atlas classes, showed notable seasonal variation in its influence on surface temperatures, with the highest contributions during summer and autumn, and comparatively lower influence in spring and winter. In summer, subtle differences in land use types, such as industrial areas, dense residential zones, and green urban spaces, become more thermally pronounced due to high solar radiation and peak energy use. These contrasts amplify microclimatic variability, making land use classification a critical predictor of surface temperature patterns (Rao et al., 2023). During autumn, the lingering thermal inertia of impervious surfaces, combined with declining vegetation activity, maintains land-use-related heterogeneity, explaining the continued high influence in this season. In spring, the moderate temperatures and increasing vegetation activity partially offset land-use contrasts, reducing their relative contribution. Whereas, in winter, low solar angles and widespread anthropogenic heating homogenize the thermal landscape.

Model Efficacy, Explainability, and Prospects for Digital Twin Integration: The superior performance of the convolutional neural network highlights the importance of deep learning for modeling high-resolution and spatially heterogeneous urban climate processes. The use of explainable AI (XAI) techniques to quantify variable contributions enhanced interpretability, helping to reveal non-obvious seasonal interactions, even with comparatively less data, that traditional models could not capture.

Although this study does not implement a digital twin framework, the combination of microscale thermal mapping, seasonal modeling, and interpretable deep learning establishes conceptual foundations for future urban “thermal digital twins”. Such systems could integrate dynamic data streams and real-time model outputs to monitor and anticipate neighborhood-scale heat behavior.

4.4. Implications for thermal mitigation and urban planning

The results highlight the need for seasonally adaptive urban design strategies. Vegetation, particularly tree canopy, is most effective during warm months and should be prioritized in dense urban areas. Zoning and land-use planning must support mixed and green land uses to enhance thermal resilience. Winter findings highlight the importance of energy-efficient building design and the management of anthropogenic heat emissions, complementing land-cover-focused interventions. The observed variability across seasons highlights the need for context-specific urban design interventions rather than one-size-fits-all strategies.

By integrating microscale thermal characterization, land-use analytics, and interpretable deep learning, this study provides a refined understanding of the drivers of urban surface temperatures. These insights support climate-sensitive planning, targeted heat mitigation, and the long-term goal of developing data-driven urban digital twins that can guide continuous, adaptive management of urban microclimates.

5. Conclusions

Overall, the study advances the scientific understanding of urban thermal behavior by providing a granular and seasonally explicit characterization of urban surface temperature dynamics. It conducted a microscale analysis of seasonal urban thermal dynamics in the Bologna municipality using a grid-based framework that integrated satellite-derived surface temperature, urban morphology and socioeconomic aspects. By accounting for both spatial and seasonal dynamics, the findings provide a foundation for developing geographically targeted heat mitigation strategies that can inform sustainable urban planning and climate resilience. The combined use of unsupervised clustering and deep learning-based explainability revealed both stable spatial patterns and pronounced seasonal transitions in LST, underscoring the combined influence of built form, vegetation, and human activity.

The clustering results identified four thermally and environmentally distinct landscape categories that remained thematically consistent but shifted spatially across seasons. The persistent thermal prominence of densely built-up zones and the cooling role of tree-covered areas reaffirm the critical importance of surface characteristics in shaping urban heat exposure. The observed seasonal transitions further demonstrate that thermal environments are temporally dynamic, emphasizing the need for planning responses that adapt to intra-annual variation. The deep learning model performed relatively better than traditional regressors and facilitated the seasonal quantification of variable contributions, confirming built surface as the dominant driver and revealing meaningful seasonal fluctuations in the roles of vegetation, land-use type, and population density. These insights suggest that mitigation strategies must be season-specific rather than uniform throughout the year.

Despite these advances, the limitations of this case study should be acknowledged. Remote sensing inputs, while high-resolution, cannot fully capture fine-scale heterogeneity such as tree canopy structure, irrigated vegetation, or rooftop greenery. The lack of detailed management data limits assessment of seasonal vegetation functioning, and the socioeconomic dimension was simplified to population density, omitting broader factors that shape vulnerability and adaptive capacity. Additionally, the temporal mismatch among the predictor datasets (2018–2020) and the downscaled 10 m LST (2021) may introduce minor inconsistencies. However, urban morphology and land use are largely quasi-static over this period. Validation of the downscaled LST was performed against Landsat 30 m LST from the same source, rather than independent ground measurements. While this approach is common in thermal downscaling studies, future work could strengthen verification using independent in-situ or higher resolution thermal data. The urban atlas and morphological zones were represented using ordinal encoding, where the assigned numerical values served as class identifiers and are inherently nominal rather than ordinal. In future studies, alternate encoding approaches like one-hot encoding could be evaluated and compared to assess the sensitivity of model performance and feature interpretation for the representation of nominal categorical variables. Addressing these limitations will require integrating higher-frequency and more detailed biophysical datasets, expanding socioeconomic indicators, and conducting comparative assessments across cities with contrasting climates and urban forms. Scenario-based modeling of projected land-use change also represents a valuable direction for understanding future thermal risk.

Within this context, the proposed framework represents a digital-twin–compatible analytical component, rather than an operational digital twin system. It provides a structured, interpretable modeling approach that can contribute to the future development of urban digital twin architectures once coupled with dynamic data assimilation and real-time updating mechanisms.

CRediT authorship contribution statement

Priyanka Rao: Writing – review & editing, Writing – original draft, Visualization, Validation, Methodology, Investigation, Formal analysis, Data curation, Conceptualization. **Patrizia Tassinari:** Writing – review & editing, Software, Resources. **Daniele Torreggiani:** Writing – review & editing, Visualization, Supervision, Project administration, Funding acquisition.

Ethical reporting standards

This manuscript presents an accurate account of the work performed as well as an objective discussion of its significance. Data and their interpretations are represented truthfully in the paper. The paper contains sufficient detail and references to permit others to replicate the work. The paper does not include fraudulent or knowingly inaccurate statements.

Hazards, humans and/or animal subjects

No hazards for humans or animals were associated with the conduct of the research.

Declaration of competing interest

Neither financial nor any other substantive conflict of interest applies. No potential conflict of interest can be construed to have influenced the results or interpretation of the manuscript.

Acknowledgments

Funded by the European Union - NextGenerationEU under the National Recovery and Resilience Plan (PNRR) - Mission 4 Education and research - Component 2 From research to business - Investment 1.1 Notice PRIN 2022 PNRR (DD N. 1409 del 14/09/2022), from title [Urban green systems: integrated modeling of environmental, energy and microclimatic benefits and GHG offsetting for strengthening resilience and adaptation to climate change – GRACE (Green foR climAte resilience)], proposal code [P20229ZC79] - CUP [J53D23018250001].

Data availability

Data will be made available on request.

References

Antonopoulos, C., Trusty, A., Shandas, V., 2019. The role of building characteristics, demographics, and urban heat islands in shaping residential energy use. City Environ. Interactions 3, 100021.

Berger, C., Rosentreter, J., Voltersen, M., Baumgart, C., Schmullius, C., Hese, S., 2017. Spatio-temporal analysis of the relationship between 2D/3D urban site characteristics and land surface temperature. Remote Sens. Environ. 193, 225–243.

Bowler, D.E., Buyung-Ali, L., Knight, T.M., Pullin, A.S., 2010. Urban greening to cool towns and cities: A systematic review of the empirical evidence. Landsc. Urban Plan. 97 (3), 147–155.

Chen, Y., Shan, B., Yu, X., 2022. Study on the spatial heterogeneity of urban heat islands and influencing factors. Build. Environ. 208, 108604.

Chen, J., Zhan, W., Du, P., Li, L., Li, J., Liu, Z., Huang, F., Lai, J., Xia, J., 2022. Seasonally disparate responses of surface thermal environment to 2D/3D urban morphology. Build. Environ. 214, 108928.

Cheung, P.K., Fung, C.K., Jim, C.Y., 2020. Seasonal and meteorological effects on the cooling magnitude of trees in subtropical climate. Build. Environ. 177, 106911.

Du, S., Zhang, X., Jin, X., Zhou, X., Shi, X., 2022. A review of multi-scale modelling, assessment, and improvement methods of the urban thermal and wind environment. Build. Environ. 213, 108860.

Emilia-Romagna Regional Geoportal, 2018. 2014 - coperture vettoriali uso del suolo di dettaglio - edizione 2018. Geoportale della Regione Emilia-Romagna. URL https://geoportale.regione.emilia-romagna.it/download/dati-e-prodotti-cartografici-preconfezionati/pianificazione-e-catasto/uso-del-suolo/2014-coperture-vettoriali-uso-del-suolo-di-dettaglio-edizione-2018. (Accessed: 02 September 2025).

European Commission, European Environment Agency, 2020. Urban atlas 2018 (2017–2019), copernicus land monitoring service. http://dx.doi.org/10.2909/fb4dffa1-6ceb-4cc0-8372-1ed354c285e6, URL https://land.copernicus.eu. Version v01 r03. Citation identifier: copernicus_v_3035_10_m_ua-2018_p_2017-2019_v01_r03. Accessed: 2025-09-02.

Han, W., 2023. Analyzing the scale dependent effect of urban building morphology on land surface temperature using random forest algorithm. Sci. Rep. 13 (1), 19312.

Hu, Y., Dai, Z., Guldmann, J.-M., 2020. Modeling the impact of 2D/3D urban indicators on the urban heat island over different seasons: A boosted regression tree approach. J. Environ. Manag. 266, 110424.

Hu, D., Meng, Q., Schlink, U., Hertel, D., Liu, W., Zhao, M., Guo, F., 2022. How do urban morphological blocks shape spatial patterns of land surface temperature over different seasons? A multifactorial driving analysis of Beijing, China. Int. J. Appl. Earth Obs. Geoinf. 106, 102648.

Huang, X., Wang, Y., 2019. Investigating the effects of 3D urban morphology on the surface urban heat island effect in urban functional zones by using high-resolution remote sensing data: A case study of wuhan, central China. ISPRS J. Photogramm. Remote Sens. 152, 119–131.

LeCun, Y., Bengio, Y., Hinton, G., 2015. Deep learning. Nature 521 (7553), 436–444.

Li, H., Li, Y., Wang, T., Wang, Z., Gao, M., Shen, H., 2021. Quantifying 3D building form effects on urban land surface temperature and modeling seasonal correlation patterns. Build. Environ. 204, 108132.

Liang, Y., Cao, S., Mo, Y., Du, M., Wang, X., 2024. Characterizing annual dynamics of two-and three-dimensional urban structures and their impact on land surface temperature using dense time-series landsat images. Int. J. Appl. Earth Obs. Geoinf. 134, 104162.

Lin, L., Zhao, Y., Zhao, J., Wang, D., 2025. Comprehensively assessing seasonal variations in the impact of urban greenspace morphology on urban heat island effects: A multidimensional analysis. Sustain. Cities Soc. 118, 106014.

Liu, Y., Zhang, W., Liu, W., Tan, Z., Hu, S., Ao, Z., Li, J., Xing, H., 2024. Exploring the seasonal effects of urban morphology on land surface temperature in urban functional zones. Sustain. Cities Soc. 103, 105268.

Marey, A., Zou, J., Goubran, S., Wang, L.L., Gaur, A., 2025. Urban morphology impacts on urban microclimate using artificial intelligence–a review. City Environ. Interactions 100221.

Meili, N., Manoli, G., Burlando, P., Carmeliet, J., Chow, W.T., Coutts, A.M., Roth, M., Velasco, E., Vivoni, E.R., Fatichi, S., 2021. Tree effects on urban microclimate: Diurnal, seasonal, and climatic temperature differences explained by separating radiation, evapotranspiration, and roughness effects. Urban For. Urban Green. 58, 126970.
O'brien, R.M., 2007. A caution regarding rules of thumb for variance inflation factors. Qual. Quant. 41 (5), 673–690.
Rao, P., Gupta, K., Roy, A., Balan, R., 2021a. Spatio-temporal analysis of land surface temperature for identification of heat wave risk and vulnerability hotspots in indo-gangetic plains of India. Theor. Appl. Climatol. 146 (1), 567–582.
Rao, P., Singh, A., Pandey, K., 2021b. Time-series analysis of open data for studying urban heat island phenomenon: a geospatial approach. Spat. Inf. Res. 29 (6), 907–918.
Rao, P., Tassinari, P., Torreggiani, D., 2023. Exploring the land-use urban heat island nexus under climate change conditions using machine learning approach: A spatio-temporal analysis of remotely sensed data. Heliyon 9 (8).
Rao, P., Tassinari, P., Torreggiani, D., 2024a. Evaluating land use indices contribution for super-resolving surface temperature: An ablation study. In: IGARSS 2024-2024 IEEE International Geoscience and Remote Sensing Symposium. IEEE, pp. 4040–4043.
Rao, P., Tassinari, P., Torreggiani, D., 2024b. A framework analyzing climate change, air quality and greenery to unveil environmental stress risk hotspots. Remote. Sens. 16 (13), 2420.
Rao, P., Tassinari, P., Torreggiani, D., 2024c. Unveiling climate dynamics: An in-depth analysis of temperature anomalies in Italian climatic regions. In: IGARSS 2024-2024 IEEE International Geoscience and Remote Sensing Symposium. IEEE, pp. 3889–3892.
Rao, P., Torreggiani, D., Tassinari, P., Rötzer, T., Pauleit, S., Rahman, M.A., 2025. Do urban green spaces cool cities differently across latitudes? Spatial variability and climatic drivers of vegetation-induced cooling. Sustain. Cities Soc. 106513.
Salvati, A., Coch Roura, H., Cecere, C., 2015. Urban morphology and energy performance: the direct and indirect contribution in mediterranean climate. In: PLEA 2015 Architecture in (R) Evolution–31st International PLEA Conference–Bologna 9-11 September. Building Green Futures, pp. 1–8.
Singh, A., Bruzzone, L., 2022. Mono-and dual-regulated contractive-expansive-contractive deep convolutional networks for classification of multispectral remote sensing images. IEEE Geosci. Remote. Sens. Lett. 19, 1–5.
Singh, A., Bruzzone, L., 2025. Wavelet-based deep generative framework for super resolution of low-resolution labeled maps and weak-supervised learning. IEEE Trans. Geosci. Remote Sens. 63, 1–14.
Singh, A., Göhner, C.S., Stendardi, L., Claus, M., Cuozzo, G., Jacob, A., Castelli, M., 2025. A transformer-based convolutional regressor to include SAR backscatter signals in monitoring alpine grasslands. IEEE Geosci. Remote. Sens. Lett..
Song, Y., Xu, H., Liu, T., Xu, J., Song, X., 2025. Linking spatiotemporal variations in urban land surface temperature to land use and land cover: A case study in hangzhou city, China. Ecol. Indic. 173, 113336.
Talukdar, S., Naikoo, M.W., Rihan, M., Mohammad, P., Rahman, A., et al., 2024. Seasonal dynamics of land surface temperature and urban thermal comfort with land use land cover pattern in semi-arid Indian cities: Insights for sustainable urban management. Urban Clim. 57, 102105.
Tehrani, A.A., Veisi, O., Delavar, Y., Bahrami, S., Sobhaninia, S., Mehan, A., et al., 2024. Predicting urban heat island in European cities: A comparative study of GRU, DNN, and ANN models using urban morphological variables. Urban Clim. 56, 102061.
Wang, Q., Wang, X., Zhou, Y., Liu, D., Wang, H., 2022. The dominant factors and influence of urban characteristics on land surface temperature using random forest algorithm. Sustain. Cities Soc. 79, 103722.
Wong, L.P., Alias, H., Aghamohammadi, N., Aghazadeh, S., Sulaiman, N.M.N., 2017. Urban heat island experience, control measures and health impact: A survey among working community in the city of kuala lumpur. Sustain. Cities Soc. 35, 660–668.
Xu, Y., Identifying the dominant seasonal drivers of land surface temperature on xiamen island: an urban functional zone perspective. Front. Environ. Sci. 13, 1661441.
Xu, X., Qiu, W., Li, W., Huang, D., Li, X., Yang, S., 2022. Comparing satellite image and GIS data classified local climate zones to assess urban heat island: A case study of guangzhou. Front. Environ. Sci. 10, 1029445.
Yang, Y., Li, X., Pan, X., Zhang, Y., Cao, C., 2017a. Downscaling land surface temperature in complex regions by using multiple scale factors with adaptive thresholds. Sensors 17 (4), 744.
Yang, Y., Zhang, X., Lu, X., Hu, J., Pan, X., Zhu, Q., Su, W., 2017b. Effects of building design elements on residential thermal environment. Sustainability 10 (1), 57.
Yuan, B., Zhou, L., Hu, F., Wei, C., 2024. Effects of 2D/3D urban morphology on land surface temperature: Contribution, response, and interaction. Urban Clim. 53, 101791.
Zhang, X., Estoque, R.C., Murayama, Y., 2017. An urban heat island study in nanchang city, China based on land surface temperature and social-ecological variables. Sustain. Cities Soc. 32, 557–568.
Zhang, Q., Guan, Y., Wu, X., Zhang, J., Li, R., Lin, K., Wang, Y., 2025. Revealing the dynamic effects of land cover change on land surface temperature in global major bay areas. Build. Environ. 267, 112266.
Zhang, L., Nikolopoulou, M., Guo, S., Song, D., 2022. Impact of LCZs spatial pattern on urban heat island: A case study in wuhan, China. Build. Environ. 226, 109785. http://dx.doi.org/10.1016/j.buildenv.2022.109785.
Zhang, Y., Wang, X., Ye, Y., Wang, L., Zhang, Y., Qin, W., Chi, Y., Liu, G., Yao, S., 2025. Nonlinear relationships and interaction effects of urban built environment on urban vitality based on explainable machine learning. City Environ. Interactions 100244.
Zhao, Y., Chen, Y., Li, K., 2025. Revealing the impacts of 3D urban morphology on surface temperature considering geometry heterogeneity, component contribution, and scale effect. Sustain. Cities Soc. 119, 106093.
Zhou, J., Liu, S., Li, M., Zhan, W., Xu, Z., Xu, T., 2016. Quantification of the scale effect in downscaling remotely sensed land surface temperature. Remote. Sens. 8 (12), 975.
Zhou, R., Xu, H., Zhang, H., Zhang, J., Liu, M., He, T., Gao, J., Li, C., 2022. Quantifying the relationship between 2D/3D building patterns and land surface temperature: Study on the metropolitan shanghai. Remote. Sens. 14 (16), 4098.
Zou, L., Tian, F., Liang, T., Fensholt, R., He, T., Schaepman-Strub, G., 2025. Topographic effects on vegetation greening and area expansion in global alpine zones under climate change. Int. J. Appl. Earth Obs. Geoinf. 142, 104727.